

# The effect of binding energy and resolution in numerical simulations of the common envelope binary interaction

Roberto Iaconi <sup>1,2\*</sup>, Orsola De Marco <sup>1,2</sup>, Jean-Claude Passy <sup>3,4†</sup> and Jan Staff <sup>5</sup>

<sup>1</sup>*Department of Physics & Astronomy, Macquarie University, Sydney, Australia*

<sup>2</sup>*Astronomy, Astrophysics and Astrophotonics Research Centre, Macquarie University, Sydney, Australia*

<sup>3</sup>*Argelander Institute für Astronomie, Bonn Universität, Bonn, Germany*

<sup>4</sup>*Max-Planck-Institut für Intelligente Systeme, Tübingen, Germany*

<sup>5</sup>*College of Science & Mathematics, University of the Virgin Islands, USVI, USA*

## ABSTRACT

The common envelope binary interaction remains one of the least understood phases in the evolution of compact binaries, including those that result in Type Ia supernovae and in mergers that emit detectable gravitational waves. Only few simulations have been carried out to date and often their results are taken at face value. In this work we continue the detailed and systematic analysis of 3D hydrodynamic simulations of the common envelope interaction aimed at understanding the reliability of the results. Our first set of simulations replicate the 5 simulations of Passy et al. (a  $0.88 M_{\odot}$ ,  $90 R_{\odot}$  RGB primary with companions in the range  $0.1$  to  $0.9 M_{\odot}$ ) using a new AMR gravity solver implemented on our modified version of the hydrodynamic code ENZO. The higher resolution achieved around the RGB core and the companion results in smaller final separations. We also carry out 5 identical simulations but with a  $2 M_{\odot}$  primary RGB star with the same core mass as the Passy et al. simulations, isolating the effect of the envelope binding energy. With a more bound envelope all the companions in-spiral faster and deeper though relatively less gas is unbound. We additionally find that for the  $2 M_{\odot}$  primary with a  $0.6 M_{\odot}$  companion, the higher the resolution, the smaller the final separation and the larger the fraction of unbound envelope gas. This suggests that simulations with a heavier companions may not be entirely converged and that interactions between companions and a  $2 M_{\odot}$  RGB primary may readily end in a merger. We finally discuss our simulations in the context of similar simulations from the literature that include the effects of recombination energy.

**Key words:** stars: AGB and post-AGB - stars: evolution - binaries: close - hydrodynamics - methods: numerical

## 1 INTRODUCTION

The common envelope (CE) interaction (Paczynski 1976; Ivanova et al. 2013) is a binary interaction that leaves behind a compact binary or a stellar merger. After Roche lobe overflow the mass transfer becomes unstable and the companion is engulfed in the envelope of the primary after which the orbital distance is quickly and greatly reduced. The CE interaction is likely the main channel of formation of most compact binaries. Compact binary white dwarfs, neutron stars and black holes have likely gone through one or more CE events during their evolution (but see Hirai 2017 for a possible alternative scenario). These systems can merge at a later time, generating Type Ia supernovae, gamma ray bursts (Fryer et al. 2007) and the emission of detectable gravitational waves (Abbott et al. 2016).

Many transients may be due to CE (and other binary interaction) events (e.g., MacLeod et al. 2017; Blagorodnova et al. 2017). Explaining these transients necessitates a reasonable theoretical description of the CE interaction and CE observations in turn provide a validation of the simulations (Galaviz et al. 2017). This synergy of simulations and observations has only become recently possible with the advent of wide and deep time-resolved surveys (e.g., the Palomar Transient Factory, Law et al. (2009), or the Catalina Real time Transient Survey, Drake et al. (2009)), which have started to detect these fast and elusive events.

Reconciling observed rates of these phenomena with our theoretical understanding of what causes them is in the hand of population synthesis models (e.g., Osłowski et al. 2011, Belczynski et al. 2016, Ablimit et al. 2016). These models use prescriptions of how the CE interactions transforms binaries into compact systems. The prescriptions provide, for example, the post-CE separation, which impacts the time-scale for the object to merge. These prescriptions are mostly *ad hoc*. A *holy grail* of CE simulations is therefore to

\* E-mail: roberto.iaconi@mq.edu.au

† Alexander-von-Humboldt fellow

provide prescriptions on how final orbital separation depends on system parameters, but simulations have not been sufficiently accurate to do so.

The CE rapid in-spiral is an intrinsically 3D interaction very difficult to study analytically or with 1D numerical models. Various numerical work have tried to tackle this difficult problem (e.g., Terman et al. 1994, Sandquist et al. 1998, Sandquist et al. 2000, Ricker & Taam 2012, Passy et al. 2012, Nandez et al. 2015, Nandez & Ivanova 2016, Kuruwita et al. 2016, Ohlmann et al. 2016a, Ohlmann et al. 2016b, Iaconi et al. 2017) using different numerical techniques (e.g., grid-codes, SPH, unstructured mesh), stellar and orbital setups and including a range of physical ingredients (though by necessity very little physics is included in these simulations). Iaconi et al. (2017) compared and contextualised different past simulations though the diversity of the techniques and the lack of sufficient coverage of parameter space has made their conclusions partial. Here we continue the effort of comparing simulations by adding to the corpus of simulations that can inherently be compared to each other and that can reveal numerical effects such as those due to resolution, or the effect of using point masses instead of bodies with a given size. These effects plague all simulations and tend, in our opinion, to be under-reported in simulation papers.

One of the main problems with CE simulations is that they are by and large unable to unbind the CE (e.g., Sandquist et al. 1998, P12, Ohlmann et al. 2016a), something that at least some systems in Nature must be able to do since we observe post-CE close binaries. Recently, simulations including the effect of recombination energy of hydrogen and helium have been able to unbind the envelope in some cases (Nandez & Ivanova 2016). However, we and others have questioned whether all of the recombination energy should be utilised to eject the envelope or whether some should leak out on account of the low opacities of recombined material (Harpaz 1998; Iaconi et al. 2017). Without understanding the fraction of recombination energy that can be used to do work, it is likely that using the entire recombination energy budget overestimates the amount of unbound gas, though not including any of it likely underestimates it.

In this paper we carry out a range of simulations similar to those carried out by P12, but with a more bound envelope. The giant is this time a  $2.0 M_{\odot}$  RGB star with the same core mass as the  $0.88 M_{\odot}$  giant used by P12. The envelope is therefore more massive and more compact. While such an envelope could be more difficult to eject, it may also induce the orbit to shrink farther, thereby mining more orbital energy and ejecting more mass. Hence the fraction of unbound envelope for a more bound envelope cannot be easily predicted. We also carry out tests with additional resolutions to perform a convergence test.

This paper is structured as follows: in Section 2 we describe the numerical setup. In Sections 3 and 4 we analyse the conservation properties of our numerical algorithms and the convergence status of our simulations, respectively. In Section 5 we analyse our results, focusing on the evolution of the orbital separation (Section 5.1) and on the dynamics of the envelope ejection (Section 5.2). Our discussion is presented in Section 6, starting with some considerations on the frequency of mergers inside the common envelope (Section 6.1), continuing with the binding properties of the envelope at the end of the in-spiral (Section 6.2) and ending with the action of the gravitational drag on the envelope gas (Section 6.3). Finally, we summarise and conclude in Section 7.

## 2 HYDRODYNAMICS SIMULATIONS' SETUP

All simulations are carried out with our modified version of the multi-dimensional hydrodynamics and  $N$ -body grid-based code ENZO (O'Shea et al. 2004, Bryan et al. 2014). For details on the numerical technique and the equations solved in our particular version of the code, see P12 and Passy & Bryan (2014). We use adaptive mesh refinement (AMR) with different levels of refinement; cells are split by a factor two along each dimension, according to the density in the cell.

We use two different 1D stellar models. The first is exactly the same as the one used by P12 and Iaconi et al. (2017): a star with a zero-age main sequence mass of  $1 M_{\odot}$ , evolved to the red giant branch (RGB) with the stellar evolution code EVOL (Herwig 2000) until its core mass reached  $0.39 M_{\odot}$ , with a total mass of  $0.88 M_{\odot}$  and a radius of  $83 R_{\odot}$ . The second model is a  $2 M_{\odot}$  zero-age main sequence star, modelled using the stellar evolution code MESA (Paxton et al. 2011, Paxton et al. 2013, Paxton et al. 2015). We stop the evolution on the RGB once the core has reached a mass of  $0.40 M_{\odot}$ , an almost identical core mass as for the first model. At this point, the RGB star has a total mass of  $1.97 M_{\odot}$  and a radius of  $66 R_{\odot}$ . The density profiles of the stabilised models for each resolution used are shown in Figure 1 and compared to the one-dimensional profile obtained with the stellar evolution code.

The primary stars have been modelled in 1D, mapped and stabilised in the ENZO grid following the same procedure used by P12 and Iaconi et al. (2017). Additionally, as suggested by Staff et al. (2016a), we use a smoothing length equal to three times the smallest cell length in all our simulations, to achieve better energy conservation. In Table 1 we summarise the most relevant initial and final parameters of the simulations, where  $M_1$  is the mass of the primary,  $M_c$  is the mass of the primary's core,  $R_1$  is the radius of the primary,  $M_2$  is the mass of the companion,  $a_i$  is the initial separation between the core of the primary and the companion and  $a_f$  is the final separation. We have carried out 4 sets of simulations:

(i) SIM1 to SIM5 reproduce those of P12, except for the fact that in this case we use AMR and smoothing length of 3 times the smallest cell length (see above) instead of 1.5 (in this way the smoothing length has the same physical size in both simulations, namely  $2.53 R_{\odot}$ ). This set of simulations is used both to test the effect of AMR on the results of P12 and to provide a direct comparison with our set of simulations carried out with a more massive primary.

(ii) SIM6 to SIM10 aim to study the effect of a more compact and massive envelope on the outcome of the CE interaction. We use the  $1.97 M_{\odot}$  star in an initial setup similar to SIM1-SIM5, with the same five companion masses, placed on the primary's surface and in circular orbit at the beginning of the simulations. No rotation has been given to the primary.

(iii) SIM11 and SIM12 are similar in all aspects to SIM9, except that they are carried out with additional AMR levels: 4 and 6, respectively. These simulations serve as a resolution test. We note that the minimum cell size of  $0.05 R_{\odot}$  in SIM12 is just larger than the core size (see Fig. 1), though it is smaller than the presumed companion radius if the companion is a main sequence star ( $R_2 = 0.66 M_{\odot}$  for  $M_2 = 0.6 M_{\odot}$ ). Even the smoothed potential radius, at  $0.15 R_{\odot}$ , is smaller than the main sequence radius of the companion. This means that the simulation allows some gas to interact with the companion when instead, for the case of a main sequence star, this gas would either be in a disk around the companion, or have accreted onto it.

(iv) Finally, SIM13, SIM14 and SIM15 are used to evaluate con-

ID	$M_1$	$M_c$	$R_1$	$M_2$	$a_1$	Domain size	Top grid resolution	Levels of refinement	Min. cell size	Boundary conditions	$a_f$	Mass inside the computational domain	Mass in the original volume of the primary	Unbound mass
	( $M_\odot$ )	( $M_\odot$ )	( $R_\odot$ )	( $M_\odot$ )	( $R_\odot$ )	( $R_\odot$ )	(cells/side)	(#)	( $R_\odot$ )		( $R_\odot$ )	(%)	(%)	(%)
SIM1	0.88	0.39	83	0.1	83	431	128	2	0.84	outflow	3.1	94	55	3
SIM2	0.88	0.39	83	0.15	83	431	128	2	0.84	outflow	3.4	86	35	4
SIM3	0.88	0.39	83	0.3	83	431	128	2	0.84	outflow	7.3	72	18	7
SIM4	0.88	0.39	83	0.6	83	431	128	2	0.84	outflow	12	59	12	10
SIM5	0.88	0.39	83	0.9	83	431	128	2	0.84	outflow	17	49	6	9
SIM6	1.97	0.39	66	0.1	66	431	128	2	0.84	outflow	2.2	98	88	1
SIM7	1.97	0.39	66	0.15	66	431	128	2	0.84	outflow	1.8	97	87	2
SIM8	1.97	0.39	66	0.3	66	431	128	2	0.84	outflow	1.6	94	70	4
SIM9	1.97	0.39	66	0.6	66	431	128	2	0.84	outflow	1.8	81	47	10
SIM10	1.97	0.39	66	0.9	66	431	128	2	0.84	outflow	2.8	78	13	10
SIM11	1.97	0.39	66	0.6	66	431	128	4	0.21	outflow	0.67	52	4	15
SIM12 <sup>1</sup>	1.97	0.39	66	0.6	66	431	128	6	0.05	outflow	0.87	84	28	13
SIM13	0.88	0.39	83	0.6	83	4310	128	2	8.4	periodic	21	100	6	N/A <sup>2</sup>
SIM14	0.88	0.39	83	0.6	83	4310	128	4	2.1	periodic	11	100	10	N/A <sup>2</sup>
SIM15	0.88	0.39	83	0.6	83	4310	128	6	0.5	periodic	10	100	12	N/A <sup>2</sup>

<sup>1</sup> The simulation has not been run until the minimum final separation was reached due to its computational cost.

<sup>2</sup> Due to the larger computational domain, the expanding layers of the envelope, with a decreasing density, are in contact with the hot vacuum for a much longer time and heated up, something that unbinds more gas. Therefore, to avoid misleading numbers, we do not report the amount of mass unbound.

**Table 1.** Initial parameters and final results of the simulations performed for this publication. Masses at the end of the simulations are expressed as a percentage of the initial envelope mass.

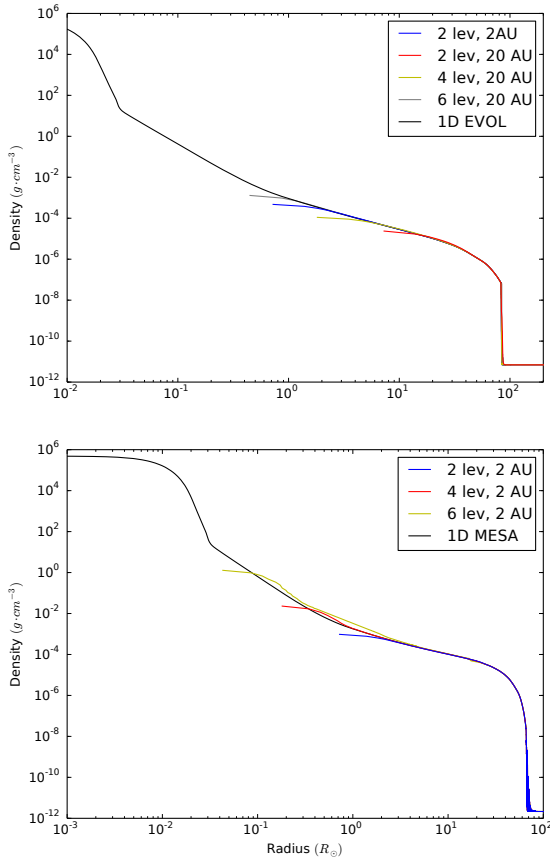


**Figure 1.** Upper panel: density profiles for the 1D EVOL model of the  $0.88 M_\odot$  giant, SIM1-SIM5, SIM13, SIM14 and SIM15. Lower panel: density profiles for the MESA model of the  $1.97 M_\odot$  giant, SIM6-SIM10, SIM11 and SIM12.

servation of energy and angular momentum. In this case we use the same physical setup of SIM4, but a larger simulation domain of 20 au per side to contain all the expanding envelope for the entire time of the CE interaction. We also use periodic boundary conditions, so that no hot *vacuum* can escape the computational domain. Given the size of the computational domain we expect the periodic boundary conditions to affect minimally the outcome of the CE interaction.

### 3 ENERGY AND ANGULAR MOMENTUM CONSERVATION

With mass flowing out of the computational domain it is difficult to check the conservation properties of our simulations. Various expedients have been devised by Iaconi et al. (2017), from using a larger domain to accounting approximately for lost mass and energy by measuring the flow of mass and energy through the domain boundary. In this work, as explained in Section 2, we carried out SIM13-SIM15 with a simulation domain able to contain the envelope for the entire time of the rapid in-spiral and with periodic boundary conditions (see Table 1), so that even small outflows of hot “vacuum” gas (low mass but high thermal energy) can be accounted for. The results for the conservation of energy are shown in Figure 2, where in the upper panel we compare the total energy as a function of time for the three simulations, while in the lower panel we show the various components of the energy for SIM15, that has a resolution similar to that of the two main sets of simulations (SIM1-SIM5 and SIM6-SIM10).

We find that energy is well conserved on the time-scale of the interaction for all the refinement levels used. All the three curves show on average a slow decrease of the total energy over time, the values of the total energy at 300 days differ by 0.1%, 0.4% and 0.2% from the initial values ( $\simeq 4.4 \times 10^{48}$  erg) for SIM13, SIM14 and SIM15, respectively. We also observe fluctuations during the three simulations, wider in the case of SIM15. At their maximum these fluctuations measure 0.1%, 0.23% and 4.5% of the initial

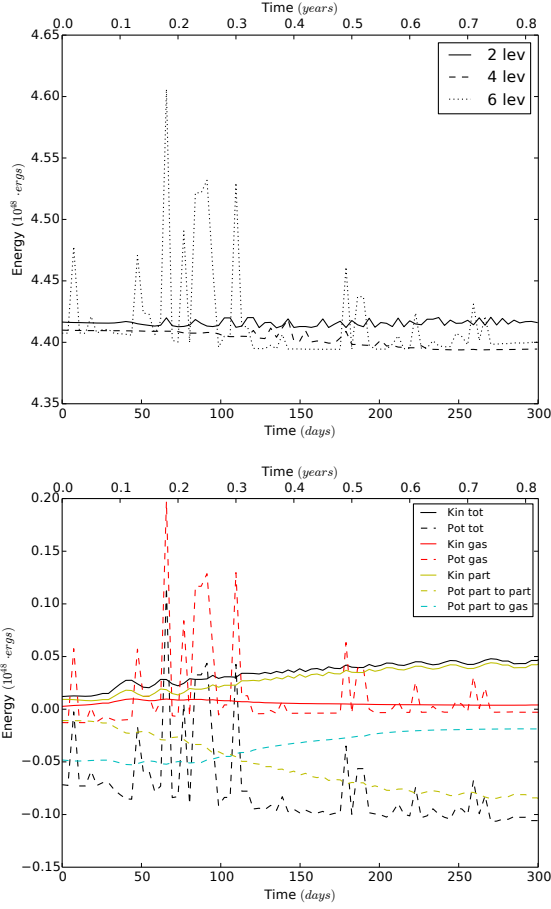


**Figure 2.** Upper panel: Total energy as a function of time for SIM13-SIM15. Lower panel: components of the energy as a function of time for SIM15. Note that total energy, total thermal energy and gas thermal energy are not plotted as the gas thermal energy dominates over all the other components due to the presence of a large amount of hot *vacuum*. Its value is constant at  $\sim 4.47 \times 10^{48}$  erg for the entire simulation.

energy values for SIM13, SIM14 and SIM15, respectively. From the lower panel of Figure 2 it is possible to observe that all the components of the energy have minor fluctuations (including thermal energy, not included in the plot) except for the potential energy of the gas, that is generating the large fluctuations in the total energy. These fluctuations are the result of approximations when AMR grids are rearranged between one top-grid time-step and another. These spikes in the potential energy of the gas take place at the boundaries between one AMR level of refinement and another and are always contained inside a single cell. These glitches in the grid rearrangement are not affecting the simulations' outcomes.

In Figure 3 we plot the the angular momentum along the  $z$  axis for SIM13-SIM15 (upper panel) and the various components of the  $z$  angular momentum for SIM15 (lower panel). Angular momentum components along the  $x$  and  $y$  axes have negligible values. Note that adopting periodic boundary conditions does not ensure angular momentum conservation: gas exiting the computational domain re-enters it from the opposite side, but with the same velocity vector, therefore with a different angle between radius and velocity vectors. Nevertheless, both mass and velocities of the gas leaving and re-entering the domain are negligible. Therefore, this does

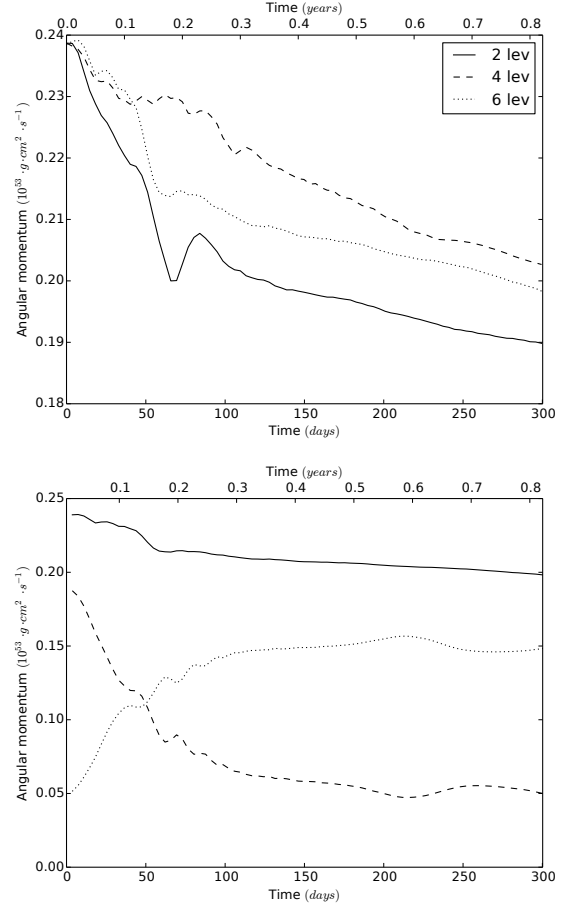


**Figure 3.** Upper panel: total angular momentum along  $z$  with respect to the centre of mass of the system as a function of time for SIM13-SIM15. Lower panel: components of the angular momentum as a function of time for SIM15: gas (dotted line), particles (dashed line), total (solid line).

not affect the estimate of the total angular momentum we carry out below.

We find that, on the time-scale of the interaction angular momentum is conserved to 21%, 15% and 17% for SIM13, SIM14 and SIM15, respectively. Where the initial value for the  $z$  angular momentum measured in the computational domain is  $\simeq 2.4 \times 10^{52} \text{ g cm}^2 \text{ s}^{-1}$ . The conservation over the first 100 days of the simulation (by which time the in-spiral has terminated) is about  $\sim 10\%$  for all three simulations.

This level of angular momentum conservation is not satisfactory and may impact the results to an extent. A loss of angular momentum may lead to more compact objects or more bound gas and it may also cause second order effects like a stronger gravitational drag. The issue of angular momentum conservation in grid codes remains a pressing one. To control angular momentum non-conservation effects we have run SPH simulations alongside grid simulations (see for example P12 and Iaconi et al. 2017). SPH simulations conserve angular momentum to a far greater level of precision, usually below 1%. We have never observed large differences in simulation outputs between identical grid and SPH simulations that could be ascribed to a lesser angular momentum conservation observed in grid simulations (usually at the 10% level). Therefore, we doubt that the conclusions of this paper would be significantly altered by the issue of the angular momentum non-conservation.

The degree of angular momentum non-conservation in the current simulations is only slightly worse than what is observed in previous simulations, including with other codes: Sandquist et al. (1998) measured a non-conservation of angular momentum at the 10% level over the 800 days of their simulation. Interestingly most of the non-conservation happened for them over the early part of their simulation, where the in-spiral takes place. In our simulations instead, the total angular momentum has a steady decline. We ascribe this worse-than-usual behaviour to the AMR aspect of the simulation, but we defer an investigation to future work.

#### 4 CONVERGENCE

A common problem of CE numerical simulations is the lack of convincing convergence tests. This is brought about by the enormous computational expense of these simulations. Convergence tests need sets of at least three simulations at regularly increasing spatial resolution. Though there is no specific limit one should increase the resolution by in convergence tests, very small resolution increments may not show lack of convergence while instead the simulation may be unconverged. We have chosen a resolution refinement factor of two so that the total number of cells increases by a factor of 8 (or a factor of 2 in each of 3 dimensions).

Another difficulty is the fact that resolution is not the only aspect of convergence. For example, the smoothing length<sup>1</sup> of our point masses can also alter the outcome of a simulation. Finally, convergence can sometimes be achieved by one of the simulation's outputs (e.g., final separations) but not another (e.g., unbound mass).

We start by noticing that the final separation in SIM13-15, which have progressively better resolution, seems to level off at  $10 R_{\odot}$ , displaying convergent behaviour. SIM4 is not identical to SIM13-15 because of the different boundary conditions, but it is similar. Its final separation ( $12 R_{\odot}$ ) is only slightly larger than for SIM14 ( $11 R_{\odot}$ ) and 15 ( $10 R_{\odot}$ ) while its resolution is intermediate ( $0.84 R_{\odot}$  vs.  $2.1$  and  $0.5 R_{\odot}$ , respectively). Though this is not a perfect convergence test we conclude that for the lighter of the two primaries the final separation has converged.

This may not be so for the case of the heavier primary. To check convergence in our simulations we compare SIM9, SIM11 and SIM12, carried out with 2, 4 and 6 levels of refinement (Table 1) and the same base grid resolution. The evolution of the orbital separation and the cumulative unbound mass as a function of time for the three simulations are shown in Figure 4.

Looking at Figure 4 (upper panel) we see that, in the first part of the rapid in-spiral, SIM9 and SIM11 have a similar behaviour, while SIM12's orbit decays faster. This is due in part to differences in the distribution of the initial AMR sub-grids. For larger maximum levels of refinement the central regions of the star near the point-mass particle and around the companion (once mass starts accumulating in its potential well) are resolved on smaller length-scales. The presence of smaller cells around the companion in the first part of the in-spiral is in particular relevant to its outcome, in fact a better sampling generates a more realistic drag. The clear difference between SIM9 and SIM11 on the one hand and SIM12 on

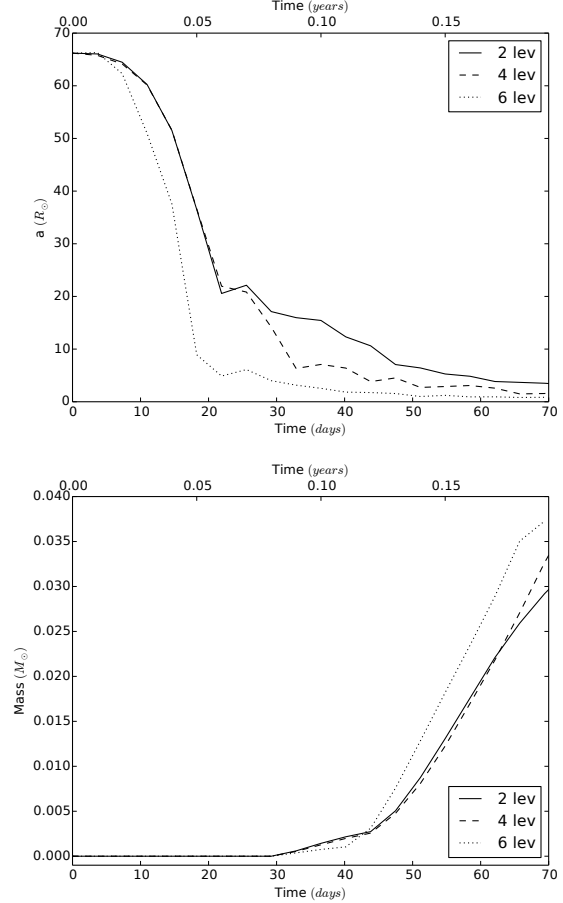


**Figure 4.** Upper panel: evolution of the separation,  $a$ , between the two particles representing the core of the primary and the companion for SIM9, SIM11 and SIM12. Lower panel: cumulative unbound mass for SIM9, SIM11 and SIM12, estimated with the same method used for the bottom panels of Figure 9 and 10. In both the panels we limit the abscissa range to 70 days, the maximum time reached by SIM12, and the line corresponding to the maximum refinement level used in the simulations is shown in the legend.

the other is that two extra grid levels provide the extra refinement around the companion, which prompts a faster in-spiral early in the simulation. Both the different distribution of the grids and the increased maximum density around the point-masses can be appreciated in Figure 5.

At the end of the simulations the orbital separation is smaller for more resolved simulations, a behaviour similar to that observed for the SPH code PHANTOM by Iaconi et al. (2017) and the behaviour is convergent (the difference is smaller between the two more resolved simulations). We only show the behaviour for 70 days because SIM12, the most resolved of the three could not be evolved for as long as the other two due to the fact that the time-step needed to satisfy the Courant condition became impossibly small. Additionally, at larger resolution, also the cumulative unbound mass recorded during the simulations is larger, displaying a similar behaviour to the orbital separation evolution (Figure 4, lower panel). Here too the high resolution simulation, unbinds more mass earlier, in line with its in-spiral being steeper, and likely caused by a strong gravitational drag at the hand of a more resolved companion-gas interaction. For now we can say that in more re-

<sup>1</sup> The smoothing length refers to the size scale by which we smooth the point mass potential to prevent it from reaching arbitrarily large values. This is different from the smoothing length in SPH simulations. When SPH simulations utilise point masses, as those carried out by Iaconi et al. (2017) do, the potential smoothing length is often called the “softening length”.

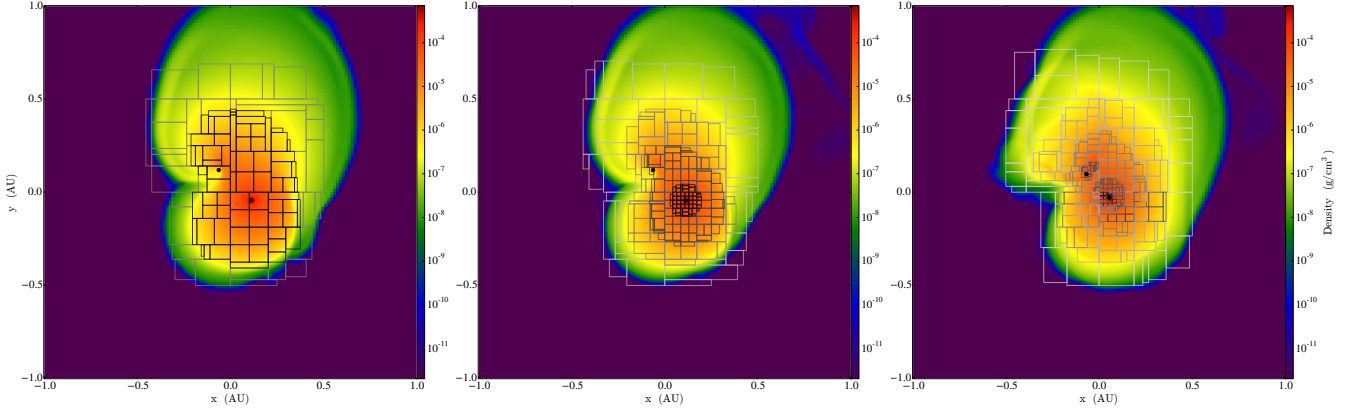


**Figure 5.** Density slices perpendicular to the  $z$  axis in the orbital plane at 15 days for SIM9 (left panel), SIM11 (centre) and SIM12 (right panel). The borders of the different refinement levels are overlotted.

solved simulations we unbind slightly more mass. This behaviour is the same of our PHANTOM simulations in Iaconi et al. 2017, which allow a precise computation of the unbound mass value and show convergent behaviour for the unbound mass at increasing number of particles.

In conclusion, we do not expect the results of our simulations to change dramatically with increased resolution, but we point out that none of these simulations is technically converged.

## 5 SIMULATIONS' RESULTS

Having assessed the conservation and convergence properties of our simulations, we now review the results.

### 5.1 The post in-spiral orbital separation

The main physical effect driving the in-spiral is the gravitational drag exerted by the envelope of the primary on the primary's core and companion (Ricker & Taam 2012). Gravitational drag depends mainly on three factors: the density of the gas surrounding the companion (and the core), the velocity of the companion with respect to the envelope gas and whether the companion speed is subsonic or supersonic (e.g., Ostriker 1999). Determining the factors that play a major role during the simulations' in-spiral is a difficult task, because it is difficult to calculate the magnitude of the different effects in the proximity of the companion (Staff et al. 2016b; Iaconi et al. 2017). The expectation is that a star that is both more massive and more compact should generate a larger gravitational drag compared to a lighter and larger one, therefore yielding a faster in-spiral and a smaller final separation.

In Figure 6 (upper panel) we show the evolution of the separation in SIM1-SIM5. We compare these to those of P12 for the  $256^3$  ENZO simulations (their Figure 4; which had a cell size of  $1.7 M_\odot$ , compared to our smallest cell size of  $0.84 M_\odot$ ). We observe that the trend of the curves for different companion masses is the same, with the most massive companions in-spiralling faster at the beginning of the interaction but reaching a larger stable separation.

In our simulations we start with an initial separation slightly smaller than P12,  $83 R_\odot$  vs.  $85 R_\odot$ , due to small differences in how the initial model becomes stable in different grids. However, even accounting for this initial offset, we find that the separation

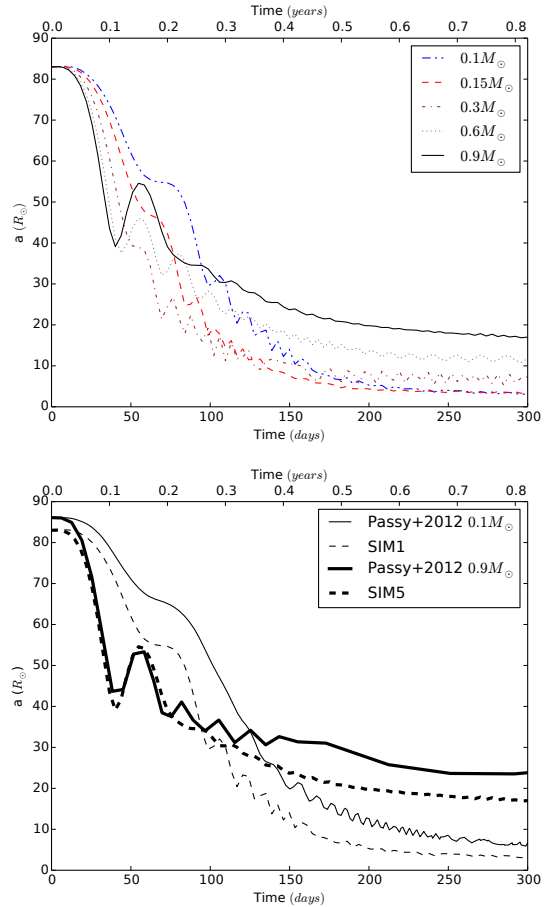


**Figure 6.** Upper panel: evolution of the separation,  $a$ , between the two particles representing the core of the primary and the companion for SIM1-SIM5. Lower panel: comparison of the evolution of the separations between this work and P12 for the least and most massive companions.

during the initial part of the in-spiral tends to evolve differently with decreasing companion's mass. At lower companion masses the uniform grid separation is larger than for the AMR grid (Figure 6, lower panel). This could be an effect of the different numerics (we solve the particles' gravity using the new solver introduced by

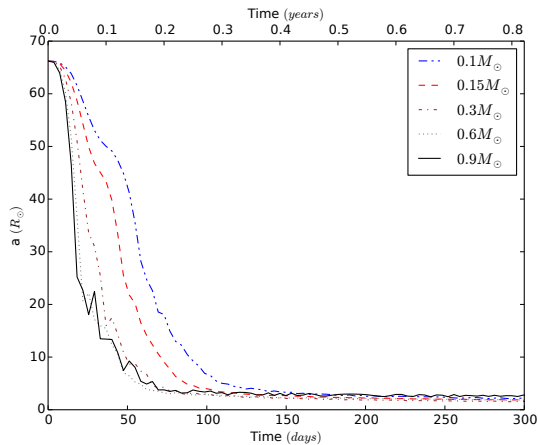


**Figure 7.** Evolution of the separation,  $a$ , between the two particles representing the core of the primary and the companion for SIM6-SIM10.

Passy & Bryan 2014) but more likely of the different resolutions, which result in a slower in-spiral and a weaker interaction between companion and primary’s envelope/core for the P12 simulations. The different resolutions also results in different final separations, with our more resolved, new simulations having smaller final separations (lower panel of Figure 6 and Figure 8). We also remark here that we adopt a larger smoothing length with respect to the grid simulations of P12 (see Section 2). This may partially affect the final separation for SIM1 and SIM2, where the companions in-spiral deeper, closer to the region where the gravity of the point-mass particle is smoothed. However, the final separations obtained for SIM1 and SIM2 are larger than the smoothing length value ( $\sim 2.53 R_{\odot}$ ). Therefore we believe that the effect of the smoothing length on the simulation outcome is minimal (this is not the case for SIM6-SIM10, see below).

We now compare the evolution of the separation between SIM1-SIM5 and SIM6-SIM10 (upper panel of Figure 6 and Figure 7). The increased gravitational drag in the case of the more massive and smaller envelope generates faster in-spirals for the entire range of companion masses. By using the same criterion as Sandquist et al. (1998) and P12 to determine the end of the rapid in-spiral phase, namely when  $-da/dt$  ( $a$  being the separation) reaches 10 % of its maximum value, we find that in SIM1-SIM5 the rapid in-spiral terminates at around 300 days. In the case of SIM6-SIM10 instead, the separation has already levelled off at 150 days for all the companions except for the least massive one, for which this happens at 190 days.

In Table 1 we list the results for the final separations obtained in our simulations, noting that now we list the values recorded at the end of the simulations rather than those at the end of the rapid in-spiral, as determined by the criterion discussed above. Additionally, in Figure 8 we plot the final separations as a function of the binary’s mass ratio for our simulations together with the observations from the publications of Zorotovic et al. (2011) and De Marco et al. (2011).

In SIM6-SIM10 the lack of an obvious  $q$ - $a_f$  correlation, observed instead in SIM1-SIM5 is likely because the separation becomes similar to the smoothing length. We used a smoothing length of 3 cells or  $2.5 R_{\odot}$ , similar to the final separations obtained. At this distance the gravitational force between the two point-masses is therefore weakened, forcing the particles to orbits larger than those they would reach in non-smoothed gravity conditions. The fi-

nal separation of the higher resolution SIM11 (see Table 1), which has a smoothing length of  $0.21 \times 3 = 0.63 R_{\odot}$ , is  $0.67 R_{\odot}$ . SIM12, with a smoothing length  $0.05 \times 3 = 0.15 R_{\odot}$ , has instead a final separation  $0.87 R_{\odot}$ , but it was not run long enough to know what the final separation would be because of enormous computational costs so that the separation has not yet levelled. Thus we can conclude that the final separation tends to decrease with resolution, and it is greatly impacted by the smoothing length. Finally, our simulations have likely not converged with respect to final separation.

Irrespective of numerical limitations, the final separations obtained in SIM6-SIM10 is much smaller and comparable to those of other simulations, most of which have binding energies similar to those of SIM6-10<sup>2</sup>. This was also concluded by Iaconi et al. (2017) using the heterogeneous set of past simulations.

## 5.2 Envelope ejection

From their comparison of all past simulations, Iaconi et al. (2017) concluded that more compact envelopes do not necessarily result in more unbound mass: despite the fact that more orbital energy is deposited in the envelope, the envelope extra “weight” leads to a similar level of unbinding. This conclusion, however was hampered by the inherent diversity of the literature simulations that were being compared and there was also a suspicion that lack of convergence was adding noise to the results. Here we provide a more solid analysis on the effect of binding energy by comparing SIM1-SIM5 with a less bound envelope to SIM6-SIM10 with a more bound one.

Gas is considered unbound if the sum of its potential, kinetic and thermal energies is greater than zero. To estimate the total amount of unbound mass, including the gas leaving the computational domain, we carried out the same interpolation used in Iaconi et al. (2017, their section 3.2).

In Table 1 we list the fraction of unbound mass in the simulations. SIM1-SIM5 unbind gas masses not dissimilar to those obtained by P12 in their SPH simulations (their table 2). Since the grid simulations performed by P12 mimicked the behaviour of SPH, we can also expect that similar amounts of unbound mass were achieved by their ENZO simulations. We therefore conclude that there are only minor differences in the unbinding of the envelope between our AMR simulations and those carried out with static, uniform grids by P12.

Comparing the results from SIM1-SIM5 and SIM6-SIM10 we can see that for companion masses  $\leq 0.3 M_{\odot}$  SIM1-SIM3 unbind approximately twice as much as SIM6-SIM8, while for companion masses  $\geq 0.6 M_{\odot}$  the unbound mass fractions are similar. Similar results were obtained by Sandquist et al. (2000), who analysed the effect of increasing the envelope mass by a factor two while keeping the core mass constant in their “Simulation 5”. They used two giants with same core mass of  $0.45 M_{\odot}$ , total masses of  $1 M_{\odot}$  and  $2 M_{\odot}$  and radii of  $243 R_{\odot}$  and  $177 R_{\odot}$ , respectively. With a relatively light companion they observed an unbound mass of 11% of the envelope for the lighter envelope and 6% for the heavier one.

SIM11 and SIM12, with a higher resolution can be compared to SIM9. A larger fraction of unbound mass seems to be promoted by higher resolution, likely, in this case, because the orbit shrinks farther, with additional release of energy. The unbound mass in SIM11 is 50 % larger than in SIM9. SIM12 has even higher resolution but it was not carried out to the completion of the in-spiral

<sup>2</sup> The only simulation that has a substantially larger binding energy is that of Rasio and Livio (1996) with a massive, compact RGB star.

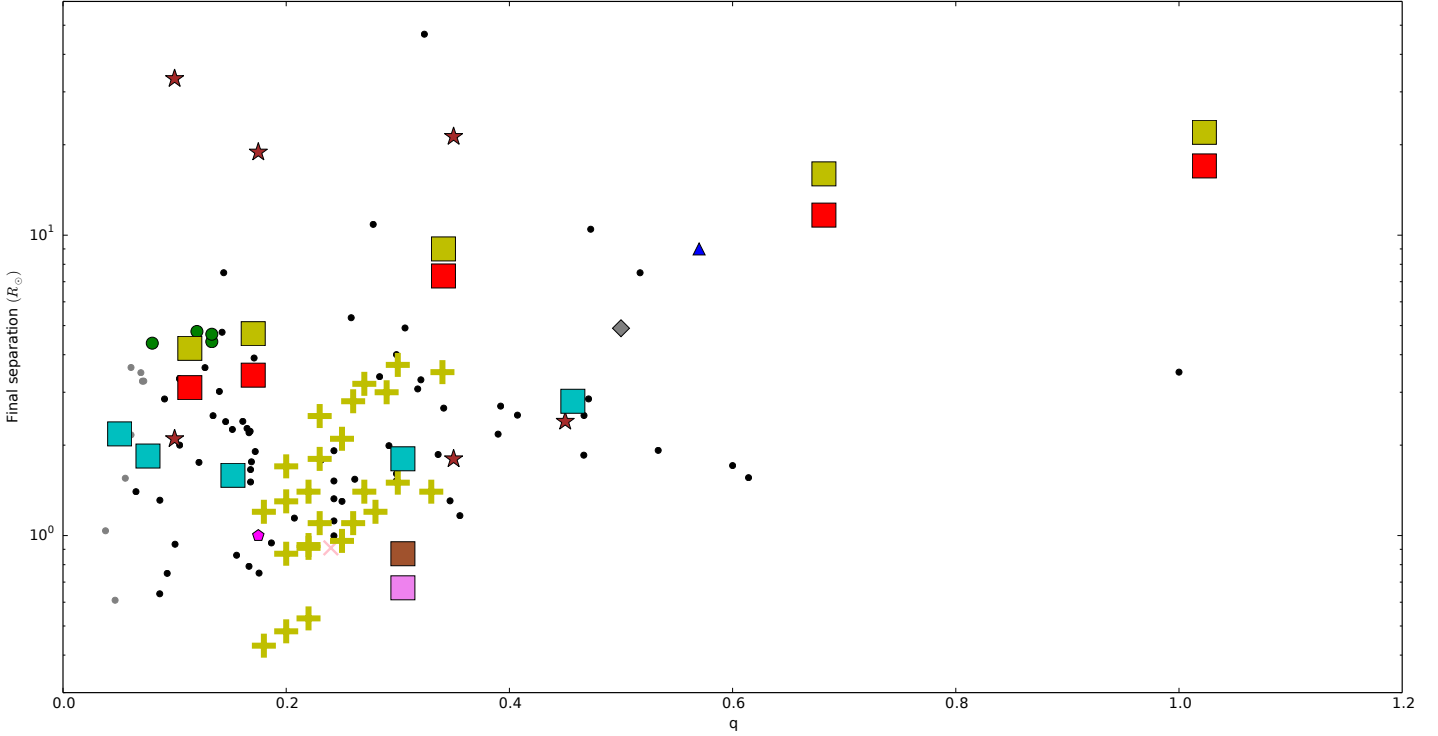


**Figure 8.** Final orbital separation vs. mass ratio  $q = M_2/M_1$  for SIM1-SIM5 (red squares), SIM6-SIM10 (cyan squares), SIM11 (brown square) and SIM12 (pink square). Past simulations are also included: P12 (yellow squares), Sandquist et al. (1998) (green circles), Ricker & Taam (2012) (blue triangle), Rasio & Livio (1996) (magenta pentagon), Ohlmann et al. (2016a) (grey diamond), Nandez et al. (2015) (pink cross), Sandquist et al. (2000) (brown stars) and Nandez & Ivanova (2016) (yellow crosses). Observed final separations gathered by De Marco et al. (2011) and from Zorotovic et al. (2011) are shown as black dots. Note that in this instance we use a logarithmic scale for the separation axis.

process due to large computational times. It does seem therefore likely that the fraction of unbound mass is not converged in this simulations.

Figures 9 and 10 show that the overall behaviour of the unbinding process is similar for both sets of simulations. The unbinding process is more gradual for less massive companions and becomes more of a bursting event for larger mass companions. This can also be seen in Figure 11, where we show the geometry of the interaction and of the unbound portions of the envelope for the two comparable simulations SIM4 and SIM9 ( $M_2 = 0.6 M_\odot$ ). In all the simulations all the unbound mass is eventually pushed out of the simulation domain. The lower panels of Figures 9 and 10 show an estimate of the cumulative unbound mass outside the simulation domain. The most prominent feature is that for the 0.6 and 0.9  $M_\odot$  companions a smaller unbinding event takes place later in time and unbinds a further 1% of the envelope gas. In all cases the bulk of the unbinding is due to envelope gas being accelerated to velocities greater than the escape velocity, with only a small percentage of the mass being unbound due to heating.

Strangely, SIM4 unbinds more mass than SIM5, against the trend observed in all other simulations where the more massive companions unbind more mass. We attribute this to lack of convergence: whether a simulation is more or less converged depends on the specifics of that simulation and it is possible that SIM5 is better converged than SIM4.

The slices of Figure 11 show snapshots of the in-spiral for the two primaries (SIM4 and SIM9,  $M_2 = 0.6 M_\odot$ ) taken at similar orbital separations. The more massive primary leads to a much faster in-spiral. For the same separation SIM4 has completely pushed out of the simulation domain the first unbound layer and several orbits have been completed, while SIM9 has not yet pushed much mass outside the computational domain and has only completed a few orbits. A similar behaviour is exhibited for other companion masses.

Similarly to what observed by Iaconi et al. (2017) and in most of the previous numerical work (see e.g., Sandquist et al. 2000, Ricker & Taam 2012), we find the presence of mild bow shocks on the ejected layers of the envelope in all our simulations. Shocks form on the front of the expanding layers of the envelope that hit the layers lifted during previous orbits. Shocks are slightly stronger for our lighter primary at similar companion mass.

## 6 DISCUSSION

### 6.1 How often should low mass stars merge with their companions?

Simulations SIM6-SIM10 end up in a very compact configuration and at higher resolution the final separation is even smaller (SIM11, SIM12). A post-CE binary survives as such if the final orbital separation does not allow any mass transfer (usually this means that

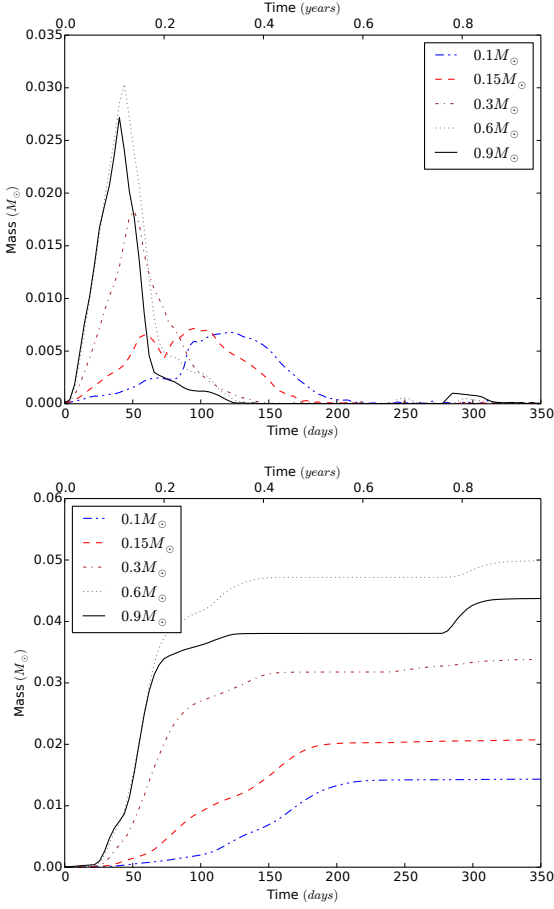


**Figure 9.** Upper panel: unbound mass inside the simulation domain for SIM1-SIM5. Lower panel: cumulative unbound mass outside the simulation domain for SIM1-SIM5. Note that the range of the abscissa has been slightly increased to 350 days to accommodate the mass that was unbound late in the simulation and therefore left the domain after the 300 days mark.

the companion is smaller than its Roche lobe radius) and if the two stars are not tidally disrupted by each other’s gravity (usually this means that the companion is outside the Roche limit of the primary’s core).

For this purpose we computed the Roche lobe radii of the companions ( $R_{\text{RL},2}$ ) at the end of simulations SIM6-SIM12 using the approximation of Eggleton (1983, Table 2):

$$\frac{R_{\text{RL},2}}{a_f} = \frac{0.49(M_2/M_1)^{2/3}}{0.6(M_2/M_1)^{2/3} + \ln[1 + (M_2/M_1)^{1/3}]} \quad (1)$$

Additionally, we computed the Roche limit for the companion disruption ( $R_{\text{lim},1}$ ) using the analytic formula from Carroll & Ostlie (2006):

$$R_{\text{lim},1} = 2.456 \left( \frac{M_1}{M_2} \right)^{1/3} R_2, \quad (2)$$

where we have assumed the companions to be main sequence stars and estimated their radii by using the mass-radius relation for low mass main sequence stars ( $R_2 = M_2^{0.8}$  all in solar units; Torres et al. 2010). Results are shown in Table 2.

The companions’ radii,  $R_2$ , are smaller than their Roche lobe radii,  $R_{\text{RL},2}$ , for SIM6-10. However, for the more resolved SIM11

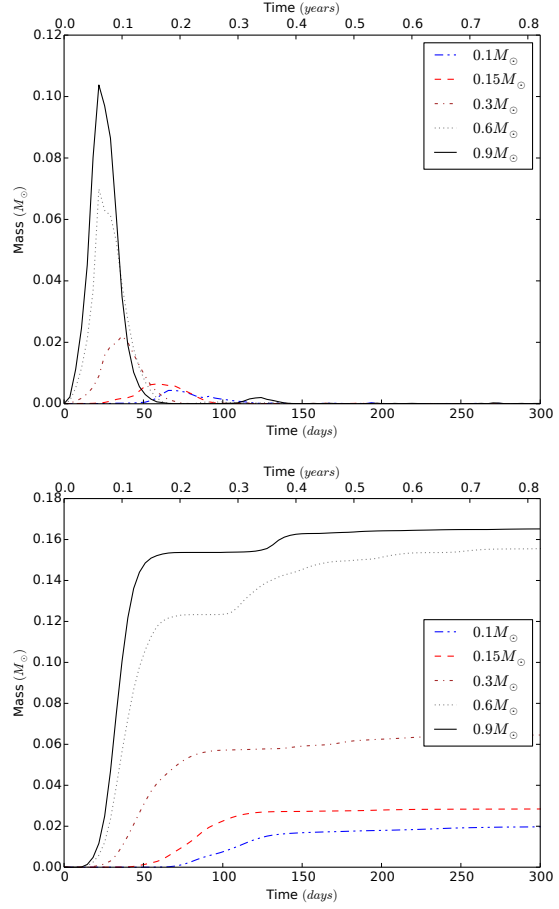


**Figure 10.** Upper panel: unbound mass inside the simulation domain for SIM6-SIM10. Lower panel: cumulative unbound mass outside the simulation domain for SIM6-SIM10.

ID	$a_f$ ( $R_\odot$ )	$M_2$ ( $M_\odot$ )	$R_2$ ( $R_\odot$ )	$R_{\text{lim},1}$ ( $R_\odot$ )	$R_{\text{RL},2}$ ( $R_\odot$ )
SIM6	2.2	0.1	0.16	0.62	0.59
SIM7	1.8	0.15	0.21	0.71	0.54
SIM8	1.6	0.3	0.38	1.02	0.57
SIM9	1.8	0.6	0.66	1.40	0.75
SIM10	2.8	0.9	0.92	1.71	1.27
SIM11	0.67	0.6	0.66	1.40	0.28
SIM12	0.87	0.6	0.66	1.40	0.36

**Table 2.** Roche limit of the primary’s core ( $R_{\text{lim},1}$ ) and Roche lobe radius of the companion ( $R_{\text{RL},2}$ ) at the end of SIM6-SIM12 ( $M_1 = 1.97 M_\odot$ ) compared to the final orbital separation ( $a_f$ ) and the mass and radius of the companion ( $M_2$  and  $R_2$ ). The higher resolution SIM11 and SIM12 could result in a merger.

and SIM12,  $R_2$  values are larger than the radius of the corresponding Roche lobe. Moreover, at such low final orbital separations, the companion is also well within the Roche limit of the primary’s core, which would result in its disruption. According to these simulations, this companion should merge with the giant core inside the CE.

Energetic considerations would suggest that a  $0.6 M_\odot$  com-

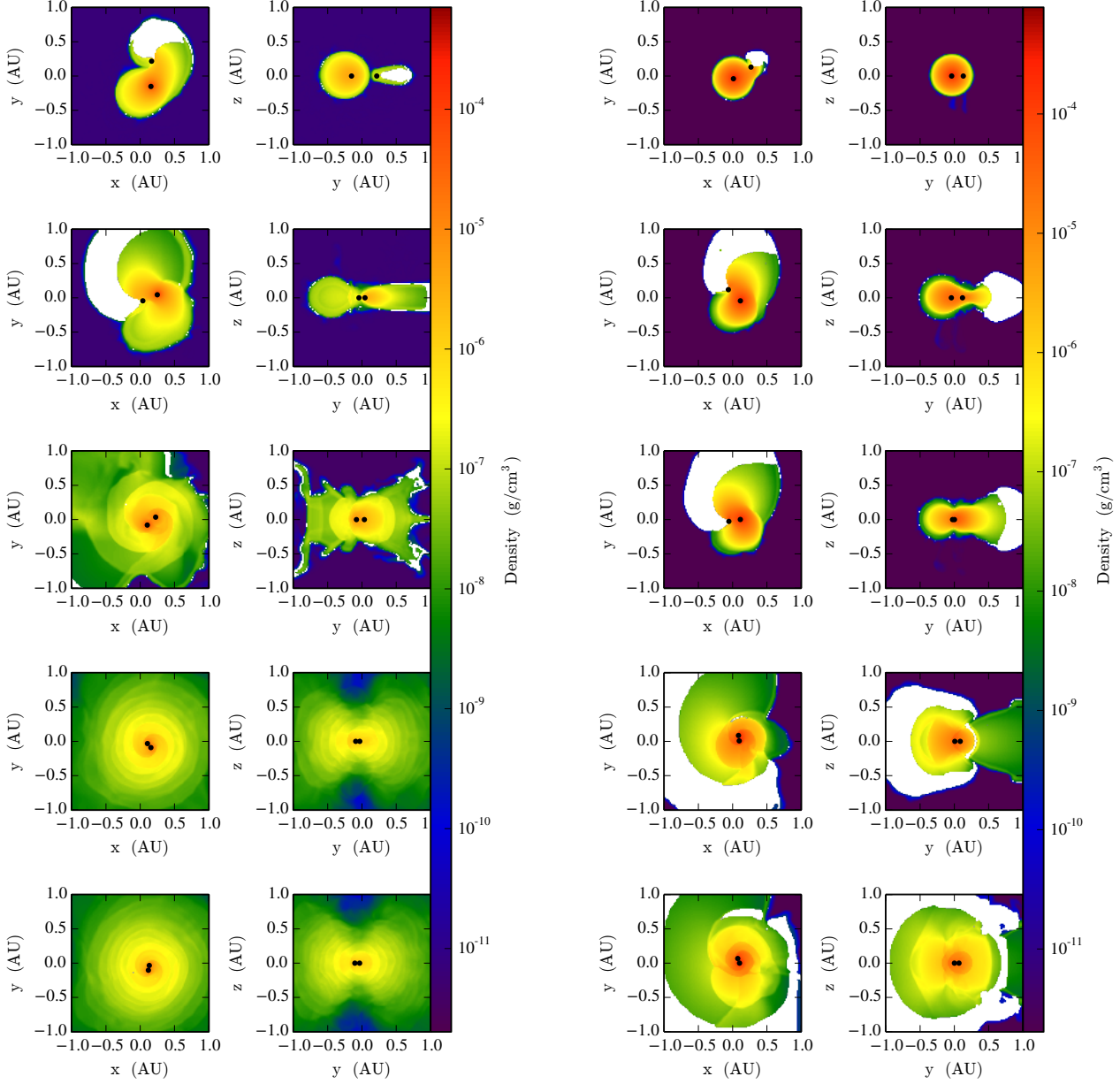


**Figure 11.** Density slices perpendicular to the  $z$  axis in the orbital plane for SIM4 (left panel, left column) and SIM9 (right panel, left column). Right columns in both the panels are the same as the left columns, but the slicing is performed perpendicular to the  $x$  axis at  $x = 0$ . Slices are captured at times when the orbital separations are approximately comparable, these times correspond to 18, 36, 76, 149, 164 days for SIM4 and 4, 15, 18, 29, 36 days for SIM9.

panion that in-spirals into the envelope of a  $2 M_{\odot}$ ,  $66 R_{\odot}$  giant to a final orbital separation such that the companion does not quite fill its Roche lobe (companion fills its Roche lobe at a separation of  $1.6 R_{\odot}$ ) would deliver enough orbital energy to unbind the envelope. The simulations, however, tell us that the orbital in-spiral would go deeper and bring the companion to merging with the core.

The simulations of Nandez & Ivanova (2016) result in smaller orbital separations overall compared to ours. Their primaries are in the range  $1.2\text{--}1.8 M_{\odot}$  with envelope radii smaller than used here (in the range  $20\text{--}60 R_{\odot}$ ). Their companion masses are in the narrow

range  $0.32\text{--}0.40 M_{\odot}$ . Among these simulations the  $1.8 M_{\odot}$ ,  $40 R_{\odot}$  simulations are the most similar to our heavy ones. Their final separation is  $1.182 R_{\odot}$ , larger than ours. This could be due to the action of recombination energy or their to low resolution of 100,000 SPH particles. Even so, the companion would likely be in Roche lobe contact ( $R_{2,\text{RL}} = 0.43 R_{\odot}$  at that separation and its radius would be  $\sim 0.4 R_{\odot}$ ), suggesting a merger. This is even more so for their simulation with a more compact,  $16 R_{\odot}$  giant. If these simulations are correct then they suggest that  $2 M_{\odot}$  giants readily merge with companions as massive as 0.3 or even  $0.6 M_{\odot}$ .

We suggest instead that the issue of reproducing the in-spiral is still open. Both orbital separation and unbinding are related to the exchange of orbital energy for total envelope energy via the drag force and all these aspects are intimately related to the simulations' resolution. Before we discuss this further, we will consider the binding status of the envelope at the end of the simulations.

## 6.2 How bound is the bound gas?

In this work we have increased the binding energy of the envelope with the aim to increase the strength of the gravitational interaction. However, there is clearly a feedback mechanism: the stronger the interaction is, the more the envelope is lifted out of the region of interaction (though not necessarily ejected), thereby weakening the gravitational interaction and reducing the ability to mine additional binding energy. Although the orbit may have delivered enough energy to match or surpass the total initial envelope binding energy, inefficiencies clearly leave much mass still bound. Inefficiencies in our code, which is adiabatic and does not radiate, equate to having ejected some mass with velocities in excess of the escape velocity and having increased the total energy of bound gas by heating and increasing its kinetic energy. In other words the average energy of the envelope can be zero after the in-spiral, but not all gas parcels have zero total energy and are therefore unbound.

The percentage value of unbound mass listed in Table 1 does not fully describe how a given simulation may have come close to unbinding the envelope: ninety per cent of the mass may still be bound, but only just. Here we investigate how close to being unbound, the *bound part* of the envelope is when the rapid in-spiral is completed, by comparing the binding energy of the *bound* envelope at the beginning and end of the simulations (Table 3).

Computing the total energy of the gas at the beginning of the simulations is trivial, since it is all contained inside the computational domain<sup>3</sup>. On the other hand, calculating any quantities that involve mass that has left the grid is complicated and approximate. Following the method devised by Iaconi et al. (2017), we determine the total energy of the *bound* gas as it crosses the domain boundary, to calculate the total energy of the bound gas that left the computational domain by the end of the simulation. The binding energy of the bound gas at the end of the simulation calculated in this way is listed in Table 3, Column 4, while listed in Columns 5 and 6 are the total energies inside and outside the computational domain, respectively, at 300 days (here we see that even a miscalculation of the energy of the bound gas that leaves the domain would not affect our conclusion). In Column 7 we can see that by the end of the simulation the binding energy of the bound gas is still a substantial fraction of the initial binding energy of the entire envelope. Hence we conclude that at the end of the simulation the bound gas is *tightly* bound rather than loosely bound.

Any energy contribution that may unbind the bound gas should therefore be substantial. We also highlight that, although the percentage of unbound mass is similar between the simulations with a lighter or heavier envelope (Table 1), the lighter envelopes are closer to unbound than the heavier ones. This is particularly evident for SIM6 and SIM7, where not only almost no mass is unbound, but also the amount of envelope removed from the initial volume of the giant is very low.

The idea of recombination energy produced in the optically thick zones of the expanding layers of the envelope as they cool down has shown promising results. Nandez et al. (2015) and Nandez & Ivanova (2016) manage to unbind more than 99% of the giant's envelope in all their simulations. According to their calculations, depending on the primary star used, the budget of recombination energy available to be injected into the envelope ( $E_{\text{rec,ini}}$ ) ranged from  $2.059 \times 10^{46}$  erg (for  $1 M_{\odot}$  stars) to  $4.676 \times 10^{46}$  erg (for  $2 M_{\odot}$  stars). If, as stated by Nandez et al. (2015) and Nandez & Ivanova (2016), recombination provides the energy necessary to achieve full unbinding, we expect that amounts of energies not dissimilar from those above could serve also in the case of our simulations. To carry out the comparison we utilise the values of  $E_{\text{f,tot}}$  shown in Table 3. We point out that the bulk of recombination takes place after the rapid in-spiral, when the layers of the envelope have lower temperature and density (see figure 11 of Ivanova & Nandez 2016). Our simulations, however, stop at the termination of the rapid in-spiral. Nevertheless, an estimate of the binding status of the envelope done at this point of the binary evolution is still valid on the time-scales of recombination, in fact only a negligible amount of energy is transferred from the orbit to the envelope. As a result the bound portion of the expanding envelope has roughly a constant total energy.

There is a net difference between the effect that the extra energy could do in the case of “light” SIM1-SIM5 and the “heavy” SIM6-SIM10. The  $E_{\text{f,tot}}$  values we obtain for SIM1-SIM5 range from  $-7.96 \times 10^{45}$  erg to  $-1.35 \times 10^{46}$  erg. These can be compared with the minimum value for  $E_{\text{rec,ini}}$  by Nandez et al. (2015) for a  $\sim 1 M_{\odot}$  primary of  $2.059 \times 10^{46}$  erg, with the result that in this case the recombination energy budget, if fully utilised, would be more than sufficient to fully unbind the envelope in all the cases. However, this is not true for SIM6-SIM10. In our second set of simulations  $E_{\text{f,tot}}$  ranges from  $-8.51 \times 10^{46}$  erg to  $-1.3 \times 10^{47}$  erg. This can be compared with the value of  $E_{\text{rec,ini}}$  of  $4.676 \times 10^{46}$  erg obtained by Nandez & Ivanova (2016) with a  $\sim 1.8 M_{\odot}$  primary. Therefore the total recombination energy would not entirely unbind the remaining portion of the envelope for all the companion masses used in this work. A similar comparison can be also carried out by using the formula proposed in section 3 of Nandez & Ivanova (2016) that calculates  $E_{\text{rec,ini}}$  as a function of the envelope mass.

## 6.3 Gravitational drag

Whether the simulations reproduce the gravitational drag correctly remains an open question. The mechanism of orbital energy an angular momentum exchange in CE simulations has been scrutinised recently by Ricker & Taam (2008), Staff et al. (2016b) and Iaconi et al. (2017). Particularly Staff et al. (2016b) argued that at lower resolutions the gravitational drag may be over-estimated, while Iaconi et al. (2017) investigated the reason why the in-spiral slows down and stabilises, concluding that there seem to be more to the gravitational drag in these simulations than is acknowledged in analytical formulations.

In a different approach MacLeod & Ramirez-Ruiz (2015) and MacLeod et al. (2017) have used 3D hydrodynamic simulations of wind tunnels to determine the factors affecting gravitational drag with particular attention to conditions affecting stars embedded in

<sup>3</sup> We do not include the effect of the companion in calculating the binding energy of the envelope at time zero, column 2, Table 3, but we do check the effect that the companion would have, column 3, Table 3.

(1)	(2)	(3)	(4)	(5)	(6)	(7)
ID	$E_i$	$E_{i,comp}$	$E_{f,tot}$	$E_{f,in}$	$E_{f,out}$	$\frac{ E_{f,tot} }{ E_i }$
	no comp.	w/ comp.	w/ comp.	w/ comp.	w/ comp.	(%)
	(erg)	(erg)	(erg)	(erg)	(erg)	
SIM1	$-2.31 \times 10^{46}$	$-2.46 \times 10^{46}$	$-1.35 \times 10^{46}$	$-1.32 \times 10^{46}$	$-2.81 \times 10^{44}$	58
SIM2	$-2.31 \times 10^{46}$	$-2.56 \times 10^{46}$	$-9.74 \times 10^{45}$	$-9.02 \times 10^{45}$	$-7.18 \times 10^{44}$	42
SIM3	$-2.31 \times 10^{46}$	$-2.83 \times 10^{46}$	$-7.96 \times 10^{45}$	$-6.90 \times 10^{45}$	$-1.06 \times 10^{45}$	34
SIM4	$-2.31 \times 10^{46}$	$-3.31 \times 10^{46}$	$-8.84 \times 10^{45}$	$-6.97 \times 10^{45}$	$-1.87 \times 10^{45}$	38
SIM5	$-2.31 \times 10^{46}$	$-3.74 \times 10^{46}$	$-1.20 \times 10^{46}$	$-8.94 \times 10^{45}$	$-3.05 \times 10^{45}$	52
SIM6	$-1.32 \times 10^{47}$	$-1.41 \times 10^{47}$	$-1.30 \times 10^{47}$	$-1.30 \times 10^{47}$	$-2.57 \times 10^{44}$	98
SIM7	$-1.32 \times 10^{47}$	$-1.45 \times 10^{47}$	$-1.28 \times 10^{47}$	$-1.27 \times 10^{47}$	$-5.03 \times 10^{44}$	97
SIM8	$-1.32 \times 10^{47}$	$-1.58 \times 10^{47}$	$-1.21 \times 10^{47}$	$-1.20 \times 10^{47}$	$-1.16 \times 10^{45}$	92
SIM9	$-1.32 \times 10^{47}$	$-1.80 \times 10^{47}$	$-1.08 \times 10^{47}$	$-1.04 \times 10^{47}$	$-3.93 \times 10^{45}$	82
SIM10	$-1.32 \times 10^{47}$	$-2.01 \times 10^{47}$	$-8.51 \times 10^{46}$	$-7.88 \times 10^{46}$	$-6.25 \times 10^{45}$	64

**Table 3.** Binding energy of the *bound* envelope at the beginning (i) and at 300 days from the beginning (f) of the simulations. We include values of  $E_i$  and  $E_f$  calculated using the values of our computational grid (columns 2, 3, 4, 5, 6). We also consider the contribution of the companion to the binding energy (columns 3, 4, 5, 6) and list the components of  $E_f$  associated with bound gas inside and outside the computational domain (columns 5 and 6, respectively). Finally, we show the percentage of bound gas energy remaining at the end of the simulations with respect to the initial value (column 7).

CE<sup>4</sup>. They concluded that the density gradient plays a role in the gravitational drag, one that is not included in analytical formalisms.

As introduced in Staff et al. (2016b), it is not easy to evaluate the gravitational drag during the rapid in-spiral in our CE simulations (but see Ricker & Taam 2008 for a specific study on CE gravitational drag). This is mainly because the behaviour of the gas around the companion is complex and the quantities needed to compute the drag are very noisy. It is easier instead to measure from the simulations the quantities that play a role in the analytical expression for the gravitational drag (e.g., Ostriker 1999). These are the density around the companion, the relative velocity of the companion and the surrounding gas and the Mach number. To calculate these physical quantities we use a control sphere of  $\sim 2.5 R_\odot$  around the companion (smaller and larger size of the control sphere do not alter the results as checked by Iaconi et al. (2017)). This is the smaller sphere we can use with a radius not enclosing only cells within the smoothing length of the point-mass. Fig. 12 shows the results of our estimates. In the left columns we plot the velocity of the companion, and the components of the gas velocity parallel and perpendicular to the companion’s direction of motion. In the right columns we plot the companion Mach number and the gas density in the control sphere. The reason to plot the velocity of the flow perpendicular to the direction of motion, not itself a quantity that influences the drag, is to have a proxy for outflow motion of the gas.

The drag goes to zero when the companion velocity is the same as that of the surrounding gas. SIM4 and SIM5 see the companion and gas velocities becoming approximately the same after the stabilisation of the orbit. However, this is not so in other simulations, showing that even after stabilisation of the orbit there is a considerable velocity contrast that should contribute to a continued drag. Bringing the gas into corotation may be something that is only

achieved by more massive companions with lower mass envelopes. No corotation is observed in SIM6-10 by the time the in-spiral is halted by reaching the smoothing length, although SIM10, with the heaviest companion is close.

The density does decrease in the vicinity of the companion at approximately the same time as the slow down of the in-spiral in simulations SIM2-5 and SIM9-10, something that would contribute to a stabilisation of the orbit, but this does not happen in the other simulations. In particular the simulations with light companions show almost no change in the density around the companion because there is very little outflow of the envelope, indicating that the in-spiral of these objects is not halted by an evacuation of the orbit.

Finally, the Mach number is effectively lower than unity in most simulations with only SIMS6 and 7 showing variable Mach values peaking above unity in the very early part of the in-spiral. We speculate that the change between supersonic and subsonic regimes in these two simulations may result in sufficient temporary reduction in gravitational drag (Ostriker 1999; Staff et al. 2016b) to halt the in-spiral in these systems, although in these two simulations the smoothing length is likely to blame for the slowing down of the in-spiral.

In Figure 13 we display the same quantities shown in Figure 12 but for SIM9 and SIM11 ( $M_1 = 1.97 M_\odot$ ,  $M_2 = 0.6 M_\odot$ ), where the only difference is a higher resolution in SIM11. The behaviours are similar for the first 40 days (as also expected by inspecting the in-spiral comparison in Figure 4). Then the companion velocity increases much more in SIM11 because the companion in-spirals deeper. The gas is not brought into co-rotation at either resolution, but at higher resolution the perpendicular gas velocity (outflow) is far more substantial, justifying the larger unbound mass fraction (Table 1). The density contrast at the time of orbital stabilisation is much lower for the more resolved simulation, possibly explaining the stabilisation itself, but also once again bearing witness to the much more efficient ejection of material for higher resolution simulations.

In conclusion the jury as to how well the gravitational drag is reproduced in CE simulations is still out. While resolution remains the number one reason why the gravitational drag may not be well

<sup>4</sup> The history of simulations attempting to understand drag and accretion numerically does not start with these contribution and relevant papers are referenced by MacLeod et al. (2017), such as the work of Hunt (1971), Taam & Fryxell (1989), Armitage & Livio (2000), Ruffert (1999), Blondin & Raymer (2012), Sánchez-Salcedo (2012) and Thun et al. (2016), to mention a representative few.

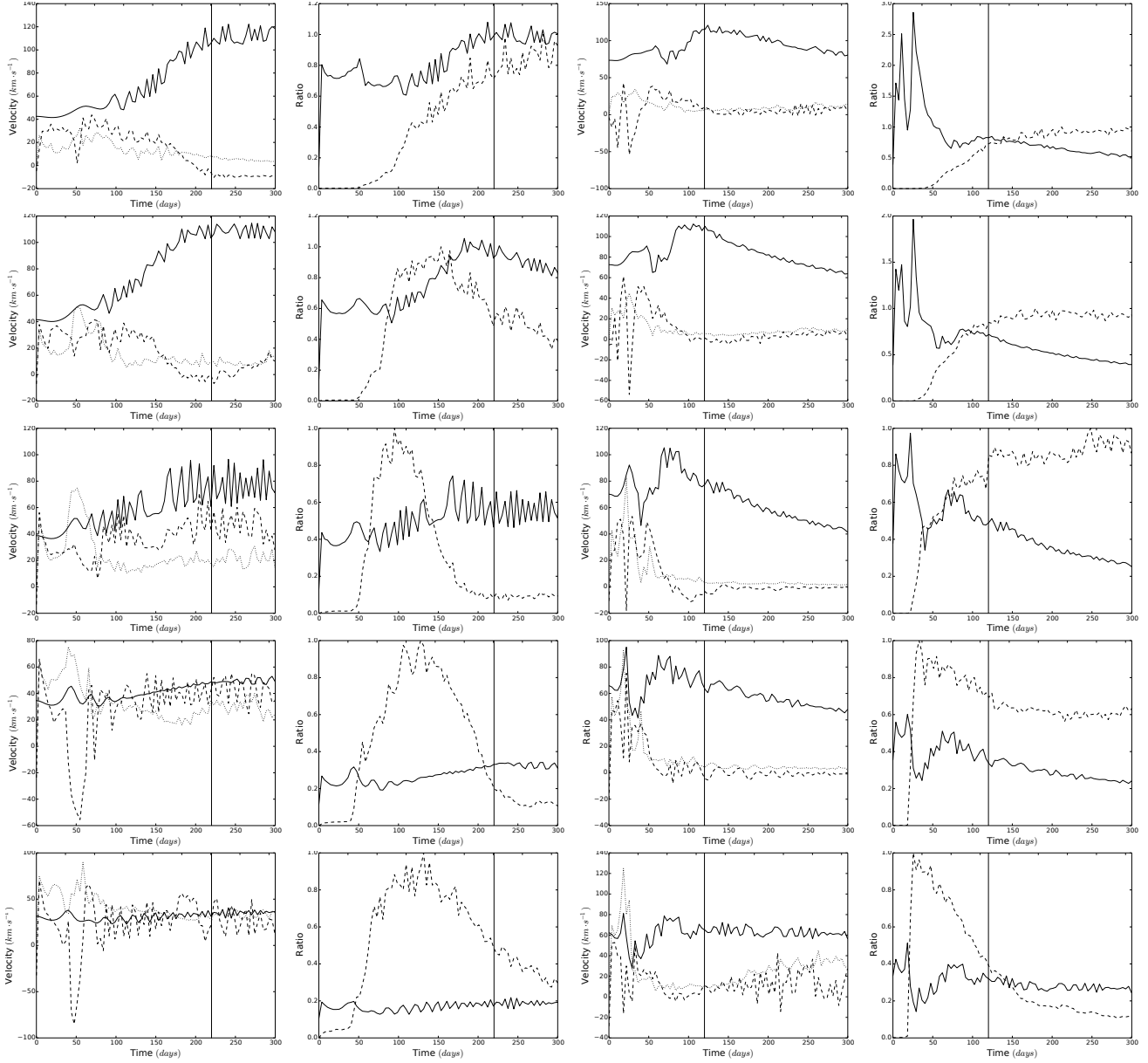


**Figure 12.** First column: companion velocity (solid line), local average gas velocity projected on the direction of the companion velocity ( $\langle v_{\text{gas},\parallel} \rangle$ , dashed line) and local average gas velocity perpendicular to the direction of the companion velocity ( $\langle v_{\text{gas},\perp} \rangle$ , dotted line). From top to bottom we plot SIM1-SIM5. Second column: companion Mach number (solid line) and normalised average gas density in the companion's proximity (dashed line). From top to bottom we plot SIM1-SIM5. Third column: same as the first, but from top to bottom we plot SIM6-SIM10. Fourth column: same as the second, but from top to bottom we plot SIM6-SIM10. The vertical lines approximately represent the points where the rapid in-spiral terminates.

reproduced, particularly when convergence tests cannot be carried out, we also see that the interplay of several physical parameters makes the in-spiral a diverse phenomenon, where similar behaviour can be brought about by different mechanisms.

MacLeod et al. (2017) argued that a density gradient makes the gravitational drag stronger. While a density gradient exists in our simulations, its impact on the drag is not considered in analytical approximation. To assess the impact of the density gradient on the drag, Iaconi et al. (2017) plotted the density of the envelope in the proximity of the companion at different moments in time, but they found it difficult to separate the underlying density gradient from the density enhancement that happens because of the presence of the companion. They concluded that the density gradient

was not clearly a factor in the in-spiral of one of their simulation, but this could be different for other simulations or at different resolutions.

Another factor that we do not take into account in simulations, nor in analytical calculations, is accretion of mass onto the companion which may also affect the strength of the drag as gas moves around the companion.

## 7 SUMMARY AND CONCLUSIONS

In this paper we have continued the systematic investigation (P12, Staff et al. 2016a, Staff et al. 2016b, and Iaconi et al. 2017) of

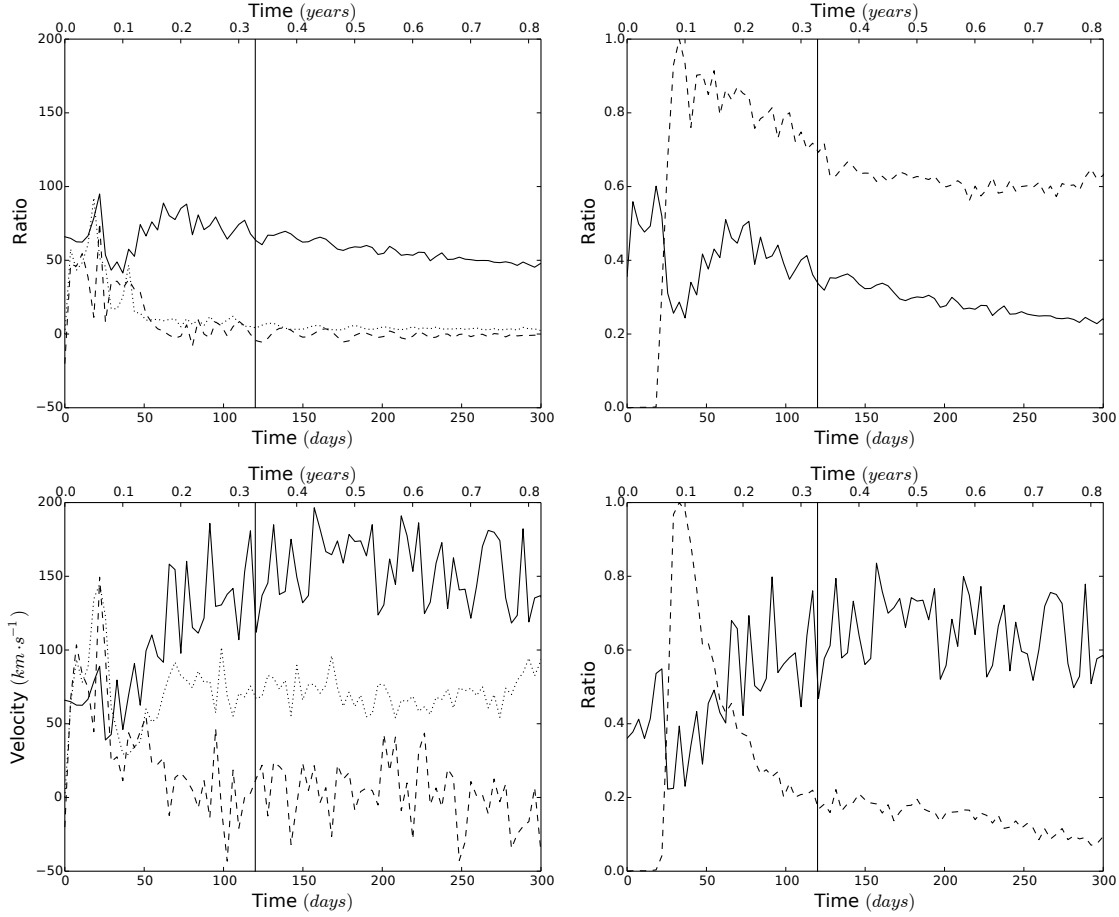


**Figure 13.** First column: companion velocity (solid line), local average gas velocity projected on the direction of the companion velocity ( $\langle v_{\text{gas},\parallel} \rangle$ , dashed line) and local average gas velocity perpendicular to the direction of the companion velocity ( $\langle v_{\text{gas},\perp} \rangle$ , dotted line) for SIM9 (top: heavy primary with  $0.6 M_{\odot}$  companion) and SIM11 (bottom: resolution twice as high). Second column: companion Mach number (solid line) and normalised average gas density in the companion's proximity (dashed line) for SIM9 and SIM11. The vertical lines approximately represent the points where the rapid in-spiral terminates.

the reliability of numerical simulations of the CE interaction by focussing on the effect of the envelope binding energy, and on resolution. We have performed two sets of simulations with the grid-code ENZO using AMR and a new gravity solver (Passy & Bryan 2014). The first set is similar to the simulations carried by P12 with ENZO in unigrid mode, while the second set models a more massive and compact primary, but with the same core mass as used by P12 and the same companions.

The new AMR simulations mimicking those carried out by P12 result in smaller final orbital separations, as well as in a stronger interaction causing a steeper fast in-spiral. We believe that these differences are due to the higher resolution achieved near the core and near the companion by the AMR technique. This higher resolution generates more bound envelopes and additionally may be causing an increase in the gravitational drag (Section 5.1). This said, the final separations reached by our more resolved simulations are not particularly different from those determined by P12, indicating that these simulations are likely reasonably well converged with respect to final separation.

The simulations with a more massive envelope than carried out by P12 result in systematically smaller final separations. However, the final separations are similar to the value of the smoothing length, pointing to un-converged behaviour. Indeed, increasing the resolution for one of the simulations (with a  $0.6 M_{\odot}$  companion),

which decreases the smoothing length, decreases the final separation. For the more resolved simulations the final separation is so small that the companion is within the Roche limit of the primary core, implying a merger (Section 5.1). Based on energy considerations a  $0.6 M_{\odot}$  companion entering a common envelope with a  $2 M_{\odot}$  star delivers enough energy to unbind the envelope before the companion merges with the core. However, what we see in our simulations is that the orbital energy is delivered inefficiently in that it contributes to kinetic energy of the envelope and to heating of layers such that either gas is unbound with higher-than-escape-velocity speeds, or raises the velocity of the gas but not enough to eject it.

The percentage of unbound envelope for the more massive primary with the  $0.1$ ,  $0.15$  and  $0.3 M_{\odot}$  companions is roughly half of that we recorded for the lighter primary with the same companions masses. For the  $0.6$  and  $0.9 M_{\odot}$  companions we instead measure a similar percentage. Also in this case resolution effects play a role, we in fact measure 50 per cent more unbound mass for twice the resolution (Section 5.2).

The question of the role of recombination energy, as tested by Nandez & Ivanova (2016) is a pressing one. In principle the addition of recombination energy can lead to envelope ejection. If recombination energy acts during the in-spiral it may lead to a wider orbital separation, which if it acts after the in-spiral has completed,

it might not. The issue of how much of this energy can be retained to do work against gravity remains an open one, but it is unlikely that all of the energy can be used. Even if the entire recombination energy budget could be used, we showed that while it would help to unbind the envelope of our lighter binaries, it would likely fail to eject those of the heavier ones (Section 6.2).

The simulations of Nandez & Ivanova (2016) with recombination energy, just like our heavier simulations (SIM6-12) without recombination energy result in very small final separations, particularly if we account for the fact that, as we discuss here, increasing the resolution of the simulations will decrease the final separation further. We therefore point out that these simulations seem to indicate that low mass RGB star readily merge with companions even if the companions are relatively heavy ( $q \lesssim 0.3$ ).

In a follow up paper (Iaconi & De Marco, in preparation) we will carry out a more in depth analysis of the simulations and of the post-CE simulations in order to determine whether the simulations carried out so far model the same type of binary that is readily observed. Only by answering this question can we then use the observations to meaningfully constrain the simulations.

## ACKNOWLEDGMENTS

RI is grateful for financial support provided by the International Macquarie University Research Excellence Scholarship. RI would also like to thank Francesco D'Eugenio for the useful discussion on angular momentum conservation. OD gratefully acknowledges support from the Australian Research Council Future Fellowship grant FT120100452. JES acknowledges support from NASA grant NNX15AP95A. This research was undertaken, in part, on the National Computational Infrastructure facility in Canberra, Australia, which is supported by the Australian Commonwealth Government and on the swinSTAR supercomputer at Swinburne University of Technology. Computations described in this work were performed using the ENZO code (<http://enzo-project.org>), which is the product of a collaborative effort of scientists at many universities and national laboratories.

## REFERENCES

- Abbott, B. P., Abbott, R., Abbott, T. D., et al. 2016, *Physical Review Letters*, 116, 061102
- Ablimit, I., Maeda, K., & Li, X.-D. 2016, *ApJ*, 826, 53
- Armitage, P. J. & Livio, M. 2000, *ApJ*, 532, 540
- Belczynski, K., Repetto, S., Holz, D. E., et al. 2016, *ApJ*, 819, 108
- Blagorodnova, N., Kotak, R., Polshaw, J., et al. 2017, *ApJ*, 834, 107
- Blondin, J. M. & Raymer, E. 2012, *ApJ*, 752, 30
- Bryan, G. L., Norman, M. L., O'Shea, B. W., et al. 2014, *ApJ*, 211, 19
- Carroll, B. W. & Ostlie, D. A. 2006, *An introduction to modern astrophysics and cosmology*
- De Marco, O., Passy, J.-C., Moe, M., et al. 2011, *MNRAS*, 411, 2277
- Drake, A. J., Djorgovski, S. G., Mahabal, A., et al. 2009, *ApJ*, 696, 870
- Eggleton, P. P. 1983, *ApJ*, 268, 368
- Fryer, C. L., Mazzali, P. A., Prochaska, J., et al. 2007, *Publications of the Astronomical Society of the Pacific*, 119, 1211
- Galaviz, P., De Marco, O., Passy, J.-C., Staff, J. E., & Iaconi, R. 2017, *ApJ Supplement Series*, 229, 36
- Harpaz, A. 1998, *ApJ*, 498, 293
- Herwig, F. 2000, *A&A*, 360, 952
- Hirai, R. 2017, *MNRAS*, 466, 3775
- Hunt, R. 1971, *MNRAS*, 154, 141
- Iaconi, R., Reichardt, T., Staff, J., et al. 2017, *MNRAS*, 464, 4028
- Ivanova, N., Justham, S., Chen, X., et al. 2013, *The Astronomy and Astrophysics Review*, 21, 59
- Ivanova, N. & Nandez, J. L. A. 2016, *MNRAS*, 462, 362
- Kuruwita, R. L., Staff, J., & De Marco, O. 2016, *MNRAS*, 461, 486
- Law, N. M., Kulkarni, S. R., Dekany, R. G., et al. 2009, *Publications of the Astronomical Society of the Pacific*, 121, 1395
- MacLeod, M., Macias, P., Ramirez-Ruiz, E., et al. 2017, *ApJ*, 835, 282
- MacLeod, M. & Ramirez-Ruiz, E. 2015, *ApJ*, 803, 41
- Nandez, J. L. A. & Ivanova, N. 2016, *MNRAS*, 460, 3992
- Nandez, J. L. A., Ivanova, N., & Lombardi, J. C. 2015, *MNRAS*, 450, L39
- Ohlmann, S. T., Röpke, F. K., Pakmor, R., & Springel, V. 2016a, *ApJ*, 816, L9
- Ohlmann, S. T., Röpke, F. K., Pakmor, R., Springel, V., & Müller, E. 2016b, *MNRAS*, 462, L121
- O'Shea, B. W., Bryan, G., Bordner, J., et al. 2004, *ArXiv Astrophysics e-prints [eprintarXiv:astro-ph/0403044]*
- Ośłowski, S., Bulik, T., Gondek-Rosińska, D., & Belczyński, K. 2011, *MNRAS*, 413, 461
- Ostriker, E. C. 1999, *ApJ*, 513, 252
- Paczynski, B. 1976, in *IAU Symposium, Vol. 73, Structure and Evolution of Close Binary Systems*, ed. P. Eggleton, S. Mitton, & J. Whelan, 75
- Passy, J.-C. & Bryan, G. L. 2014, *ApJ Supplement Series*, 215, 8
- Passy, J.-C., De Marco, O., Fryer, C. L., et al. 2012, *ApJ*, 744, 52
- Paxton, B., Bildsten, L., Dotter, A., et al. 2011, *ApJ Supplement Series*, 192, 3
- Paxton, B., Cantiello, M., Arras, P., et al. 2013, *ApJ Supplement Series*, 208, 4
- Paxton, B., Marchant, P., Schwab, J., et al. 2015, *ApJ Supplement Series*, 220, 15
- Rasio, F. A. & Livio, M. 1996, *ApJ*, 471, 366
- Ricker, P. M. & Taam, R. E. 2008, *ApJ*, 672, L41
- Ricker, P. M. & Taam, R. E. 2012, *ApJ*, 746, 74
- Ruffert, M. 1999, *A&A*, 346, 861
- Sánchez-Salcedo, F. J. 2012, *ApJ*, 745, 135
- Sandquist, E. L., Taam, R. E., & Burkert, A. 2000, *ApJ*, 533, 984
- Sandquist, E. L., Taam, R. E., Chen, X., Bodenheimer, P., & Burkert, A. 1998, *ApJ*, 500, 909
- Staff, J. E., De Marco, O., Macdonald, D., et al. 2016a, *MNRAS*, 455, 3511
- Staff, J. E., De Marco, O., Wood, P., Galaviz, P., & Passy, J.-C. 2016b, *MNRAS*, 458, 832
- Taam, R. E. & Fryxell, B. A. 1989, *ApJ*, 339, 297
- Terman, J. L., Taam, R. E., & Hernquist, L. 1994, *ApJ*, 422, 729
- Thun, D., Kuiper, R., Schmidt, F., & Kley, W. 2016, *A&A*, 589, A10
- Torres, G., Andersen, J., & Giménez, A. 2010, *The Astronomy and Astrophysics Review*, 18, 67
- Zorotovic, M., Schreiber, M. R., & Gänsicke, B. T. 2011, *A&A*, 536, A42

This paper has been typeset from a  $\text{T}_{\text{E}}\text{X}/\text{L}^{\text{A}}\text{T}_{\text{E}}\text{X}$  file prepared by the author.